Comparison of nitrous acid detection using open-path incoherent broadband cavity-enhanced absorption spectroscopy and extractive long-path absorption photometry

Sophie Dixneuf[1§], Albert A. Ruth[1*], (the late) Rolf Häseler[2✝], (the late) Theo Brauers[2⧧],
Franz Rohrer[2], and Hans-Peter Dorn[2]

[1]Department of Physics & Environmental Research Institute, University College Cork, Cork, Ireland.
[2]Institut für Energie und Klimaforschung, IEK-8: Troposphäre, Forschungszentrum Jülich GmbH, 52425 Jülich, Germany.

[§]Current address: Bioaster Technology Research Institute - Bioassays, Microsystems & Optics Engineering Unit, 40 Avenue Tony Garnier, 69007 Lyon, France

Correspondence to: Albert A. Ruth (a.ruth@ucc.ie)

✝ Rolf Häseler - passed away on 25 July 2017.
⧧ Theodor Brauers - passed away on 21 February 2014.

Abstract. An instrument based on 20 m open-path incoherent broadband cavity-enhanced absorption spectroscopy (IBBCEAS) was established at the Jülich SAPHIR chamber in Spring 2011. The setup was optimized for the detection of HONO and NO_2 in the near UV region 352-386 nm, utilizing a bright hot-spot Xe-arc lamp and a UV-enhanced CCD detector. A 2σ detection limit of 26 pptv for HONO and 76 pptv for NO_2 was achieved for an integration time of 1 min. Methacrolein has also been detected at mixing ratios below 5 ppbv. The IBBCEAS instrument's performance for HONO and NO_2 detection was compared to that of extractive wet techniques, long-path absorption photometry (LOPAP) and chemiluminescence spectrometry (CLS) NO_X detection, respectively.

1 Introduction

Photolysis of nitrous acid (HONO + hν (λ < 400 nm) → OH + NO) leads to the formation of the most important daytime oxidant in the atmosphere, the hydroxyl radical (OH). Thus HONO indirectly affects the oxidative potential of the troposphere and strongly influences degradation mechanisms of a vast variety of natural and urban pollutants. The mechanisms of HONO formation in the troposphere are still not fully understood (Calvert et al. 1994, Finlayson-Pitts et al. 2003, Ramazan et al. 2004, Liu et al. 2019). Many atmospheric studies revealed elevated HONO mixing ratios during daytime under specific conditions that cannot be fully explained (Staffelbach et al. 1997, Zhou et al. 2002a, Zhou et al. 2003, Kleffmann et al. 2003, Vogel et al. 2003, Kleffmann et al. 2005, Acker et al. 2006, Spataro and Ianniello, 2014). Although there appears to be general agreement that heterogeneous NO_2 chemistry is one of the most important sources of HONO (Harrison et al. 1994, Reisinger 2000),

modelled HONO mixing ratios are often significantly below observed values (Vogel et al. 2003, Lammel and Cape 1996). However, other sources have also been suggested (Stemmler et al. 2006, Li et al. 2012, 2014). Since the photochemistry of HONO is closely connected to that of NO_2 (Johnston et al. 1974, Aumont et al. 2003, Bröske et al. 2003, Ramazan et al.

35 2004), the in situ measurement of time-dependent HONO and NO_2 mixing ratios by monitoring both species simultaneously is particularly interesting to elucidate the natural formation processes of HONO (Kleffmann 2003). One reason for the indeterminate formation and atmospheric role of HONO is the challenge to accurately and reliably quantify this species.

A direct spectroscopic way to detect HONO is through its electronic absorption in the near UV between 320 and 390 nm (Stutz et al. 2000), or through its IR active vibrational modes (Barney et al. 2000), e.g. in the Q-branches of trans-HONO at 1263 cm^{-1}

40 (ν_3) or 790 cm^{-1} (ν_4). The cross-sections in both cases are approximately between ~2 and 6×10^{-19} cm^2/molecule. The UV region has been extensively exploited in differential optical absorption spectroscopy (DOAS) (Febo et al. 1996, Alicke et al. 2003, Stutz et al. 2010), but more recently also using cavity enhanced methodologies (Wang and Zhang 2000, Djehiche et al. 2011, Jain et al. 2011), especially incoherent broadband cavity enhanced absorption spectroscopy (IBBCEAS) (Gherman et al. 2008, Hoch et al. 2012, Wu et al. 2012, Donaldson et al. 2014, Scharko et al. 2014, Min et al. 2016, Nakashima and

45 Sadanaga 2017, Duan et al. 2018, Jordan and Osthoff 2020, and Yi et al. 2021). The mid-IR was targeted using Fourier transform (Hanst et al. 1982) and tuneable diode laser spectroscopy (TDLAS) (Schiller et al. 2001). Laser-induced fluorescence (LIF) can also be used for sensitive HONO detection, but only through the emission of OH radicals that are formed after HONO photolysis (Rodgers and Davis 1989, Liao et al. 2006, Bottorff et al. 2021).

Most non-spectroscopic (indirect) detection methods are chemical in nature. Typical approaches comprise dry (Ferm and

50 Sjödin 1985), and wetted effluent diffusion (Simon and Dasgupta 1995, Acker et al. 2006), or rotated (Oms et al. 1996, Spindler et al. 2003) denuders, HPLC/fluorescence methods (Huang et al. 2002, Takenaka et al. 2004, Beine et al. 2005), or long path absorption photometry (LOPAP) (Heland et al. 2001, Kleffmann et al. 2002). The corresponding instrumentation is generally more sensitive than spectroscopic methods, but at the same time also more susceptible to chemical interferences that can affect the selectivity and quantification of HONO (Beine et al. 2005, Kleffmann et al. 2006). In most of the chemical methods HONO

55 is sampled on humid or liquid surfaces where heterogeneous chemistry can affect HONO mixing ratios in the presence of specific interfering chemicals (Ferm et al. 1985, Spindler et al. 2003, Zhou et al. 2003, Gherman et al. 2008). Moreover, photolytic or heterogeneous formation of HONO in sampling lines are known to cause unreliable results in in situ measurements (Zhou et al. 2002a, 2002b, Rohrer et al. 2005). Therefore for studies aiming at HONO detection it is essential to compare the performance of instruments that use genuinely different approaches (Kleffmann 2007). E.g. validation studies

60 of denuder based approaches against DOAS measurements illustrated that significant discrepancies exist for daylight/illuminated conditions (Kleffmann 2007). DOAS was also compared with the LOPAP approach and several reasons for systematic differences in the acquired data were identified (Kleffmann et al. 2006).

A long open-path broad-band cavity enhanced absorption instrument was set up at the SAPHIR[1] chamber at
Forschungszentrum Jülich (Germany) in 2011, utilizing an incoherent short-arc Xe lamp as a light source (cf. Fiedler et al.
2003, Varma et al. 2009). Results of measurements to characterize its performance in the near UV through the in situ detection
of HONO and NO_2, as well as methacrolein (MACR) are presented here. Similar to the recent work by Yi et al. 2021 our
objectives in 2011 were (i) to assess the instrument's performance concerning HONO detection and validate it with the LOPAP
system available at SAPHIR, and (ii) to compare its performance concerning NO_2 detection with the local SAPHIR
chemiluminescence spectrometry (CLS) NO_X detector.

Section 2 outlines details on the experimental setup at SAPHIR in Jülich. Section 3 shows measurements of HONO,
NO_2 and MACR mixing ratio using the IBBCEAS instrument. The data are respectively compared with results from different
instruments at SAPHIR: (a) a LOPAP system (HONO), (b) a standardized chemiluminescence detector (NO_2), and (c) a proton-
transfer reaction mass spectrometer (PTRMS) (MACR). Correlation plots between individual measurements will be discussed
for three measurement days in Summer and Autumn 2011. The experiments presented here supplement a campaign on the
"Formal Intercomparison of Observations of Nitrous Acid" (FIONA) (Rodenas et al. 2013), where instruments for the detection
of HONO were compared at the EUPHORE simulation chambers in Valencia (Spain) in May 2009.

2 Experiment

IBBCEAS has been used for the detection of a variety of target species in different wavelength regions in the laboratory
(Langridge et al. 2006, Washenfelder et al. 2008, Dixneuf et al. 2009, Thalman and Volkamer 2010, Wu et al. 2009, Nakashima
and Sadanaga 2017, Duan et al. 2018) and in outdoor environments (Bitter et al. 2005, Saiz-Lopez et al. 2006, Leigh et al.
2010, Wu et al. 2012). The high sensitivity and spatial resolution of open-path IBBCEAS make this approach particularly
attractive for applications in atmospheric simulation chambers (Varma et al. 2009, Fuchs et al. 2010, Chen et al. 2011, Ashu-
Ayem et al. 2012, Hoch et al. 2012, Dorn et al. 2013, Rodenas et al. 2013). Thus an open-path IBBCEAS instrument was
developed at the Jülich SAPHIR chamber, a facility designed for the simulation of tropospheric scenarios at realistically low
mixing ratios of relevant trace species. The SAPHIR chamber is an ideal testbed for open-path IBBCEAS due to the available
comprehensive suite of standard detection methods that can be used to assess and validate the data taken with IBBCEAS. For
the experiments presented here the IBBCEAS instrument was optimized for the near-UV detection of HONO (352-386 nm),
whose identification was based on three prominent absorption bands peaking at ≈354, ≈368 and ≈384 nm (Stutz et al. 2000).
The spectral region covered also enabled the simultaneous detection of NO_2 and methacrolein.

The experimental design of the IBBCEAS instrument was similar to the one described in Refs. (Varma et al. 2009, Dorn et al.
2013, Varma et al. 2013). It comprised a transmitter and a receiver unit, each housing one of the cavity mirrors. A sketch of
the optical setup and details on experimental components are shown in Figures S1-S3 in the supplementary material. The

---

[1] SAPHIR = **S**imulation of **A**tmospheric **PH**otochemistry **I**n a large **R**eaction chamber)

transmitter unit was mounted on a concrete platform at the north end of SAPHIR (facing south). The receiver unit was located

at the south end of SAPHIR (facing north), in order to minimize exposure of the detector to potential daytime stray light. The

95   dielectric mirrors ($r = -21$ m, $R \sim 0.999$, diameter = 40 mm, Layertec GmbH) inside the mechanically stable units formed an

optical cavity with a mirror separation of ~20.4 m. Each unit was temperature stabilized with an air-to-air thermoelectric

assembly (Laird Technologies). Vertical metal plates with optical ports (Figure S3) were rigidly mounted to the concrete

support and formed the interface between the instrument's units and the chamber. Pipes connected to the two units extended

into the SAPHIR chamber through the optical ports. Due to the use of the vertical plates (sealed by o-rings) the mechanical

100   stress of the chamber's teflon wall was not imposed directly on the two optical units, which essentially decoupled the instrument

from the chamber wall and improved its long-term stability. Each unit had two ports: one pipe with 50 mm diameter and

another one with 25 mm. In each unit the wider pipe was aligned along the optical axis of the cavity reducing the contribution

of stray light to the measured signal in the receiver unit. The pipes were sealed with a high reflectivity mirror at one end and

purged with zero air at a flow rate of 1.7 dm^3 min^{-1} during measurements to protect the mirror. The narrower pipe, which was

105   sealed off during normal use of the instrument, was only used as a port for a green alignment laser (see Figure S1). The main

light source was a short-arc Xe lamp running in "hot-spot" mode. In this mode, a small plasma spot (~150 μm diameter) with

a spectral radiance of 18 W cm^{-2} sr^{-1} nm^{-1} at 400 nm was formed close to the cathode surface, improving the imaging properties

of the discharge in comparison to conventional diffuse arcs. Small random jumps of the arc position, however, required an

active stabilization of the beam direction by means of a quadrant detector. When the spot "jumped" to a specific quadrant an

110   actively controlled piezo-driven Al-mirror was used to minimise the resulting beam deviation from the optical axis of the

CEAS instrument. A telescope imaged the incoherent light into the optically stable cavity whose mirrors were aligned by two

remote-controlled high resolution positioning motors per mirror. The light transmitted by the cavity was collected by a UV-

enhanced Al-mirror and focused onto the aperture of a circular-to-rectangular fiber bundle which guided the light onto the

entrance slit (25 μm) of a (Shamrock 303i) spectrograph (f = 303mm, F/4) supplied with a 1200 grooves/mm holographic

115   grating. The light transmitted by the spectrograph was imaged onto a CCD detector cooled to –65°C. Light outside the high

reflectivity range of the cavity mirrors was optically filtered by means of a band-pass filter to avoid excessive scattering into

the spectrometer and the potential saturation of the detector. The wavelength range from 352 to 386 nm was covered with a

spectral resolution of ~0.24 nm. A sample of transmission spectra can be found in the supplementary material (Figure S4).

2.1 Measurement Procedure

120   After overnight flushing of the chamber with dry synthetic air (also referred to as "zero air" in this publication) the cavity

transmission, $I_0(\lambda)$, was measured every morning in the dark chamber before experiments commenced. Typically 300 cavity

transmission spectra with an individual acquisition time of 200 ms were accumulated during experiments, yielding a time

resolution of 1 min per measured spectrum $I(\lambda)$. The extinction coefficient $\varepsilon(\lambda)$ [cm^{-1}] was calculated according to (the left

part of) Eq. (1):

125

$$\varepsilon(\lambda) = \frac{1 - R_{\mathrm{eff}}(\lambda)}{d}\left(\frac{I_0(\lambda)}{I(\lambda)} - 1\right) = a_0 + a_1\lambda + a_2\lambda^2 + a_3\lambda^3 + a_4\lambda^4 + \sum_{i=1}^{N} n_i\sigma_i(\lambda) \qquad (1)$$

where R_{eff} represents the wavelength dependent effective reflectivity of the cavity mirrors and $d = 19.57$ m the interaction path

length per pass in the cavity (d equals the mirror separation minus the length corresponding to the mirror purge volume, see

130   supplementary material, Figure S1). $(1 - R_{\mathrm{eff}})$ comprises all effective optical losses of the cavity when filled with zero air after

purging the chamber overnight; i.e. mirror reflectivity losses, Rayleigh (and potentially) Mie scattering losses, diffraction

losses. The spatial average of the number density n_i [molecule cm^{-3}] of the absorbing species i (= HONO, NO$_2$ and MACR)

was retrieved by fitting the function on the right hand side in Eq. (1) to the measured extinction coefficient. σ_i [cm^2 molecule^{-1}] represent the absorption cross-sections of species i. The cross-sections for HONO (Stutz et al. 2000), NO$_2$ (Mérienne et al.

135   1995) and MACR (Meller et al. 1990) were converted to the spectral resolution of the spectrometer using home-made Gaussian

convolution software written in Fortran. The five fit parameters a_j (j = 0...4) in Eq. (1) belong to a fourth-order polynomial,

accounting for unspecified additional losses, such as background featureless absorption, or Rayleigh and Mie scattering that

may become relevant over time. The fitting procedure was based on least squares minimization using a singular value

decomposition (SVD) procedure (Press et al. 1986, Varma et al. 2009) in order to eliminate biases of the fit due to parameter

140   correlations. During a first test run of the SVD approach the wavelength of all cross-section reference spectra were individually

shifted to further minimize the least square sum, and the optimized wavelengths were subsequently used in SVD analyses. For

all reference spectra the typical shift was $\approx 0.10 \pm 0.05$ nm and thus within the spectral resolution of the measurement. The

absolute wavelength (e.g. used in Fig. 4) was calibrated with a low-pressure neon pen ray lamp. Reflectivity calibration issues

will be discussed in the section 4.

145   **2.2 The LOPAP Instrument**

The LOPAP instrument used in this study has been described in detail by Häseler et al. 2009 and Li et al. 2014 in the context

of several campaigns on airborne detection of HONO aboard a Zeppelin airship. Air is extracted through two sampling coils

in series where HONO is stripped into the liquid phase. In both coils the air is exposed to equal flows of a solution (0.06 M

sulphanilamide in 1 M HCl solution) in which HONO almost instantaneously reacts to forms a diazonium salt. While the first

150   coil removes HONO nearly quantitatively from the gas phase, only a fraction of other chemically interfering species are

scrubbed. The second coil, however, samples that fraction of interfering species but only the remaining small amount of

HONO. Using the difference of the signals derived from the two coils enables the influence of interfering species to be

accounted for. The air is then separated from the liquid and the solutions are separately transferred into two mixing volumes,

where a 0.8 mM solution of N-(1-naphthyl)ethylenediamine-dihydrochloride is added to generate an azodye. The azodye's

155   concentration is then determined by its optical absorption to determine HONO mixing ratios. The absorption cells for both

channels consist of long length teflon tubing, acting as a liquid core waveguide (LCW). Visible light is sent through the tubing and detected by two small spectrometers.

The entire instrument was housed in a compact 19" rack (56(w) × 60(d) × 100(h) cm^3) consisting of two "chemistry" units and one "electronics/detection unit". In order to avoid sampling artefacts in inlet lines the sampling unit was straightforwardly mounted inside SAHPIR about 0.3 m from the chamber wall at the north end and 1 m above the floor. The instrument's sampling frequency, time resolution, 3σ detection limit, 1σ precision, and accuracy of the instrument was 0.33 Hz, 4-5 min, 10 pptv, 3 pptv, and 12 %, respectively. The measurement range of the instrument can in principle be varied by the length of the absorption tubes and by the use of different absorption wavelengths for the evaluation. In this study we used an optical path length of 2.9 m.

2.3 Chemiluminescence Spectrometry NO$_X$ Detector

The NO$_X$ detector was located in a container underneath the chamber from where gas mixtures were sampled at a flow rate of 1 dm^3 min^{-1} through a teflon tube of ca. 6 m length (internal diameter 4 mm) corresponding to an approximate residence time of 1 s. NO$_2$ was converted to NO by a pulsed LED photolytic converter at 395±8 nm (Droplet Measurement Technologies, BLC) in a volume of 17 ml with a conversion efficiency of approximately 50%. The LED in the converter was consecutively switched on and off to alternately determine NO and NO$_X$ concentrations. NO was detected by a customized CLS detector (Eco Physics TR 780 (Rohrer and Brüning 1992, Fuchs et al. 2010). NO$_2$ mixing ratios were calculated using an interpolated value between two subsequent NO$_X$ measurements at a time when NO mixing ratio were measured. The instrument was calibrated using NO standard gas mixtures (2 ppmv NO in N$_2$, BOC-Linde) and gas phase titration for NO$_2$.

The fact that besides NO$_2$ also HONO is photolysed at 395 nm to yield NO was accounted for by determining the corresponding NO yield from HONO numerically from the spectrum of the LEDs. The HONO photolysis contribution to NO is less than 5% compared to that of NO$_2$. The 1σ accuracy of the chemiluminescence detector for NO$_2$ was determined to be ±7%, based on the uncertainty of ±5% of the NO standard used for the calibration and a ±5% uncertainty for the NO$_2$ conversion efficiency. The known interference of 5% towards HONO is not corrected in the final dataset and not included in this accuracy estimate.

2.4 Proton Transfer Reaction – Mass Spectrometry (PTRMS)

PTRMS was utilized to monitor methacrolein in the presence of HONO and NO$_2$. Generally the PTRMS technique relies on soft chemical ionization to detect gaseous trace components. The target species are converted to product ions through the transfer of a proton from the reagent ion, H$_3$O$^+$. The trace gases (X) are identified through the mass of the product ions usually being the protonated molecular mass (XH$^+$): H$_3$O$^+$ + X → XH$^+$ + H$_2$O. The PTRMS instruments applied here was a quadrupole mass spectrometer system (PTR-Quad-MSThe system features a switchable reagent ion source with H$_3$O$^+$, NO$^+$ and O$_2$$^+$ as precursor ions for the measurement and identification of a number of trace gases. Details on the PTRMS instrument were published earlier by Wisthaler et al. 2008.

3 Results

Measurements of time-dependent mixing ratios of HONO, NO_2 and MACR using open-path IBBCEAS were taken during Summer and Autumn 2011, and compared with those utilizing long-path absorption photometry (LOPAP), chemiluminescence

190 spectrometry (CLS) and proton transfer reaction mass spectrometry (PTRMS), respectively. The performance intercomparison study is exemplified on basis of measurements on the 11th of July and on the 5th & 6th of October 2011, when different photo-chemical scenarios were simulated. The measurements in July were carried out as part of a Jülich internal photochemistry campaign (6th June to 15th July 2011), whose goal was to study the oxidation of isoprene ($H_2C=C(CH_3)-CH=CH_2$), methacrolein $CH_2=C(CH_3)–CHO$ or methyl vinyl ketone ($CH_3-C(O)-CH=CH_2$) by hydroxyl (OH) radicals at low NO_X mixing

195 ratios (Nehr et al. 2014, Fuchs et al. 2014). In contrast, the measurements in October were specifically designed for a comparison between LOPAP and IBBCEAS under well controlled low concentration conditions with no obvious potential chemical interferences disturbing the LOPAP instrument. Generally, after cleaning and humidifying the SAPHIR chamber HONO formation by unknown photo-induced reactions on the Teflon chamber walls and degradation was studied in experiments always including light-induced and dark reactions of HONO formation or destruction – the experimental protocols

200 concerning changes in chamber conditions are given in the figure captions. The results obtained on the three days will be outlined in chronological order. The performance of the open-path IBBCEAS instrument will subsequently be discussed in the context of the different measurement condition and atmospheric scenarios together with that of the Jülich LOPAP instrument.

Figure 1

3.1 Measurements on 11 July 2011

205 Figure 1 (left panels) summarizes the time-dependent measurements of mixing ratios of HONO, NO_2 and MACR as determined by IBBCEAS (black symbols), LOPAP (red), CLS (blue) and PTRMS (green). The same color code is also used in Figures 2, 3 and 5. The vertical arrow in Figure 1 indicates the times when the cavity transmission through the clean chamber, $I_0(\lambda)$, was measured for ca. 10 min. 11 July is the only day for which the build-up of HONO was monitored during daylight conditions. The HONO mixing ratio increased after humidification of the bright chamber (for 48 min) and decreased subsequently when

210 O_3 (~40 ppbv) was introduced. At 9:15 hrs there is a marked but unexplained change in the data of HONO mixing ratios as measured by IBBCEAS in comparison to LOPAP. The increase in the noise of the IBBCEAS data occurred ca. 15 minutes before the addition of CO to the chamber at 9:30 hrs, which is neither expected to influence the HONO chemistry nor the data retrieval, even at high CO (~750 pbbv) concentrations (see Figure 1). Presently there is no obvious explanation for this behavior in the IBBCEAS measurement. Likewise the return to dark conditions at 15:33 hrs led initially to an unexpected increase of

215 the HONO mixing ratio as recorded by the LOPAP instrument, but it was also observed by the IBBCEAS measurement. This observation was also made in other campaigns and will be briefly discussed in section 4.2. NO_2 mixing ratios, as measured by CLS, increased gradually during humidification of the bright chamber and increased sharply when O_3 was introduced, followed by a more gradual increase until MACR was added to the mixture at 11:51 hrs. The jump of the NO_2 mixing ratio at 07:30

shows the effect when O_3 was added actively to the chamber. Almost all NO was oxidised to NO_2 at that time. Both CLD and
220 CEAS show this effect. The observed temporary decrease of the NO_2 concentration after the addition of MACR can be
explained by a reaction sequence following the formation of OH from HONO: The primary oxidation step of the reaction of
OH with MACR forms the peroxy methacryloyl radical ($CH_2=C(CH_3)-C(O)OO$), part of which further reacts with NO_2 to
form MPAN (peroxy methacryloyl nitrate, $CH_2=C(CH_3)-C(O)OONO_2$). MPAN is thermally unstable with a small thermal
decomposition rate of ~ 4.6×10^{-4} s^{-1} at 25°C (Roberts and Bertman 1992). Thus a thermal equilibrium is established from which
225 NO_2 is reformed after the initial MACR has been consumed (Fuchs et al. 2014).

Concentrations of NO_2 and MACR both appeared to stagnate when the roof was closed due to the absence of light-driven
photo-chemistry. Finally the purging of the chamber with synthetic air removed all trace gases from the chamber.

The experiments in October were designed to enable accurate mirror reflectivity calibration and intercomparison of LOPAP
and IBBCEAS under unperturbed condition at sub-ppbv mixing ratios of HONO. The measurements demonstrate that the
230 long-cavity IBBCEAS instrument at SAPHIR is capable of detecting HONO pptv levels without difficulty (Figures 2 and 3).

3.2 Measurements on 5 October 2011

After overnight flushing in the morning of 5 October, NO_2 was added to the chamber in steps of 250 pptv (at 6:30 hrs and
6:50 hrs), 500 pptv (at 7:10 and 7:30), and 1 ppbv (at 7:50 hrs and 8:10 hrs). After subsequent humidification for 44 min
(starting at 8:41 hrs) and the exposure to daylight at 9:27 hrs, HONO was formed at levels of up to 400 pptv. Finally, after
235 closing the chamber roof (14:23 hrs), HONO was removed by flushing with zero air (starting at 15:31 hrs). The HONO data
from the IBBCEAS and LOPAP setups, and the NO_2 data from the IBBCEAS and CLS instruments showed outstanding
agreement on that day (Fig. 2).

Figure 2

3.3 Measurements on 6 October 2011

240 It is known that the photo-enhanced formation of HONO in the SAPHIR chamber can be described by an empirical function
depending on relative humidity, solar irradiation and temperature (Rohrer et al. 2005). Minimal HONO production was thus
achieved by only humidifying the chamber for 42 min after overnight flushing with zero air. At 12:18 hrs the chamber was
exposed to daylight leading to the gradual formation based on vestiges of NO_X on the chamber wall. The variation of
temperature was limited to the natural variability. After a gradual increase the HONO mixing ratios leveled off at ca. 250 pptv
245 before the chamber was eventually closed at 16:24 hrs. The correlation between the data obtained with IBBCEAS and LOPAP
is rather satisfactory at these low levels. For NO_2 there appears to be a slight offset between data from the IBBCEAS and CLS
instruments with good overall agreement.

Figure 3

4 Discussion of Instruments' Performances

4.1 IBBCEAS Instrument

The main experimental uncertainties determining the quality of the IBBCEAS data reported here are systematic; they are: (a) the stability of the light source, (b) the in situ calibration of the mirror reflectivity, (c) the data analysis and concentration retrieval approach, and (d) the unspecified mechanical instabilities of the setup such as potential thermal drifts or deficiencies of the opto-mechanical components (Ruth et al. 2014). The latter become more critical with increasing cavity length since small changes in the optical alignment have a more severe influence on the instrument's performance; see Varma et al. 2009.

4.1.1 Lamp Stability

Short-term intensity fluctuations are due to random spatial variations of the hot spot plasma arc (small arc jumps), whose effects on the optical alignment were minimised by an active quadrant detector control unit (Varma et al. 2009). As long as intensity fluctuations of the lamp do not show any spectral dependence in the wavelength range of interest, the resulting baseline changes can in principle be accounted for in the fit of eq (1) to the measured data. If the fluctuations are however accompanied by random spectral variation, the retrieval by SVD becomes increasingly difficult. Spatial jumps that were at the compensation limit of the quadrant detector were also noted during experiments leading to uncertainties in the baselines. One of these events may have occurred e.g. on 11 July at ~9:30 hrs. Difficulties in the mixing ratio retrieval due to lamp instabilities occurred sporadically during the measurements in the Summer, but became more frequent and for longer time periods after continued use of the lamp in the Autumn. For instance the measurement on 6 Oct (Figure 3) was affected by lamp stability issues, which is a sign of electrode aging and the main cause for the hot spot plasma arc to wander into a domain where the stabilization system is unable to fully compensate for the spatial displacement.

An unexplained change in performance started approximately 20 min before the addition of 750 ppbv of CO on 11 July at ca. 9:10 hrs (Figure 1). At that time the quality of the IBBCEAS data started to worsen, while the LOPAP performance remained largely unaffected (see Figure 1). A small increase in HONO mixing ratios was subsequently observed in comparison to the LOPAP and the noise of the IBBCEAS data was increased by roughly a factor of ~2. There are no obvious reasons for this observed behavior from a (photo)chemical point of view, since at the time the gas mixture was not altered. In open path cavity setups similar behavior can in principle be caused through increased scattering due to particle formation (Varma et al. 2009), but measurements of the particle number concentration showed no significant change on this occasion. Therefore one conceivable explanation may be that the hot spot arc in the Xe lamp may have moved to a steady location on the electrode where the control unit was at its performance limit to keep the arc steady. As the quadrant detector correction signal was not recorded, this is merely a tentative explanation of the sudden change of performance. Although there was an addition of CO a short time later it is not plausible that potential impurities in the CO (purity >99.9%) gas (or chemical reactions of same) might be the cause for this observation. LED-based IBBCEAS is generally less prone to sudden changes (Gherman et al. 2008) due to the higher stability of the light source, although slow drifts are still possible (Fouqueau et al. 2020).

4.1.2 Mirror Reflectivity and Calibration Aspects

Retrieval of accurate mixing ratios by IBBCEAS requires the effective mirror reflectivity R_{eff} to be known accurately as a function of wavelength. Calibration measurements were performed a few times over the course of the measurements presented here by introducing a known amount of NO_2 into the dry SAPHIR chamber shortly after the cavity transmission of the clean

285 and dry cavity, $I_0(\lambda)$, had been recorded. The effective reflectivity was retrieved with eq (1) using the known cross-section of NO_2 and the mixing ratio from the CLS NO_X monitor (e.g. using the measurements on 5th Oct 2011 where $R_{\text{eff}} = 0.9978$ at 352 nm and $R_{\text{eff}} = 0.9986$ at 386 nm, see supplementary Figure S5). The lower limit of the absolute uncertainty (~11%) is based on the accuracy of the NO_2 cross-section (8%) and that of the NO_X measurement (7%).

The initial calibration measurement of R_{eff} was also used to determine the loss, $L_{\text{LLO}}(\lambda)$, of an anti-reflection coated optic

290 (referred to as "low loss optic", LLO), which was in turn used on a daily basis (in the morning) to determine the reflectivity in the clean chamber instead of using NO_2 as calibration gas (see also supplementary Figures S4 and S6):

$$R_{\text{eff}}(\lambda) = 1 - \left(\frac{I_{\text{LLO}}}{I_0 - I_{\text{LLO}}} L_{\text{LLO}}(\lambda) \right) \tag{2}$$

295 In the transmitter unit the LLO (R_{LLO} (375 nm) < 0.001, diameter 40 mm, parallelism 30") was moved into and out of the cavity parallel to the mirror by means of an accurate translational stage with high reproducibility. Care was taken in designing the air-tight LLO compartment (Figure S1) where the optic was "parked" when not needed. The LLO was furthermore flushed with clean dry air while in the cavity to avoid (minimize) potential changes of its optical loss. When the LLO is used over the course of a simulation experiment, i.e. in a chamber with arbitrary gas mixture, the LLO measurements yield effective

300 reflectivities that comprise extinction losses in the chamber at this particular time. Although only the R_{eff} measured each morning in the clean dry and dark chamber was used to retrieve the concentrations of the target species (eq (1)) for the entire day, repeated introductions of the LLO into the cavity over the course of the day was used for checking whether misalignments or potential drifts of the cavity had occurred.

305 ### 4.1.3 Data Evaluation

In order to judge the quality of the data evaluation an example of an IBBCEAS extinction spectrum and the corresponding fit of eq (1) to the measured data are shown in Figure 4 (uppermost panel). The data for this example were chosen because on 11 July 2011 HONO, NO_2 and MACR were simultaneously present in the chamber. The different panels in Figure 4 show the individual absorption contributions of the three species to the measured spectrum together with the polynomial background

310 determined in the fit analysis. The lowermost panel shows the fit residuals, $\Delta\varepsilon$, illustrating the appropriate use of the reference absorption spectra of the three target species in this measurement.

4.1.4 Detection Limits

For individually measured spectra a minimum extinction coefficient of 9.3×10^{-10} cm^{-1} was determined for an acquisition time of 1 min (assuming a 1:1 signal-to-noise ratio), which corresponds to $\varepsilon_{min} = 7.2 \times 10^{-9}$ cm^{-1} Hz$^{-1/2}$ (1σ). For a series of

315 measurements (see supplementary Figure S7) this translates into a measured 3σ limit of detection (LOD) of the IBBCEAS instrument for a 1 min acquisition time of ~39 pptv for HONO, ~114 pptv for NO$_2$, and ca. 510 pptv for MACR in the 352-386 nm wavelength range.

In comparison to the IBBCEAS instrument, the LOPAP instrument at SAPHIR featured a 3σ LOD of 10 pptv of HONO in 1 min. The LOD for NO$_2$ by the standardised chemiluminescence technique at SAPHIR also compares favourably with a 3σ

320 LOD of 13.4 pptv of NO$_2$ for a 1 min acquisition time with an overall accuracy of 7 % (Rohrer and Brüning 1992, Fuchs et al. 2010) (the CLS detection limit for NO is ≈6.7 pptv). Mixing ratios of volatile organic compounds such as methacrolein can be only compared to data acquired with PTRMS, whose LOD for MACR is 8.5 pptv in 1 min (accuracy 8 %).

An overview of (2σ) detection limits for HONO of previously published IBBCEAS instruments was recently given by Jordan and Osthoff 2020. The 2σ detection limit of 26 pptv for HONO in 1 min presented here compares favourably to the IBBCEAS

325 works by Gherman et al. 2008, Hoch et al. 2012, Wu et al. 2012, Donaldson et al. 2014, Scharko et al. 2014, Min et al. 2016, Nakashima and Sadanaga 2017, Duan et al. 2018, and Jordan and Osthoff 2020 - see Table 1 in the AMT article by Jordan and Osthoff 2020. It should be noted, however, that some of the quoted detection limits were established under field conditions, which bears challenges that are different from experiments with a large scale simulation chamber. The rather competitive detection limits of the current setup are a result of the substantial cavity length, despite the fact that the effective cavity mirror

330 reflectivity in this work was lower than in all other instruments reported.

Figure 4

4.2 LOPAP Instrument

In a previous DOAS-LOPAP intercomparison (Kleffmann et al. 2006) the addition of ozone triggered issues concerning the use of proper reference data in the DOAS evaluation procedure at ppbv levels of HONO. This sort of difficulty was not

335 observed with IBBCEAS at sub-ppbv mixing ratios of HONO.

However, when switching from illuminated to dark conditions the LOPAP instrument regularly showed an increase of HONO concentrations, while the IBBCEAS detector does not seem to follow this trend as strongly and reproducibly; see Figure 1 (11 July 2011) or Figure S8, for example. The systematically increasing HONO mixing ratios measured by the LOPAP instrument upon closing the roof and generating dark conditions was also observed on a few other days during the summer campaign, e.g.

340 on 10 and 15 June (see supplementary Figure S8). The reason for this behavior is not fully understood yet. An effect of the presence of organic reaction products from the oxidation of mathacrolein that cause an interference with the LOPAP technique upon stopping photolytic processes can be ruled out, because the "effect" was also observed in experiments with a clean humidified chamber solely filled with high purity synthetic (zero) air. A possible explanation may be based on the changing

homogeneous and heterogeneous production rates of HONO versus its destruction rates under bright and dark conditions. For
345 daytime conditions the steady state HONO mixing ratio is mainly determined by photolysis of a yet unknown nitrogen containing precursor adsorbed at the Teflon walls or dissolved in the surface water layer on the Teflon film versus the photolytic destruction of HONO into OH and NO. In the dark (closed) humidified chamber HONO can still be produced, but predominantly through heterogeneous reactions with formation rates being at least a factor of ~10 smaller than under illuminated conditions (i.e. with the roof open). Even though closing the roof stops efficient HONO production it also
350 eliminates the photolytical loss entirely, while HONO heterogeneous production within the aqueous phase on the chamber walls is still active (albeit its slowly decreasing efficiency). This can lead to changing the equlibrum such that the subsequent outgassing of HONO from the aqueous phase on the Teflon film can temporarily dominate the HONO production into the gas phase until the initially HONO-saturated aqueous phase also gets depleted leading to the eventual decrease in HONO mixing ratios (Karl, 2004). The inlet of the LOPAP instrument is much closer to the chamber wall (ca. 30 cm) in comparison to the
355 region probed by IBBCEAS, which averages across the whole length of the chamber near its center. Thus the effect is more likely to be apparent in the LOPAP data than in the IBBCEAS data. This tentative explanation of the observed trend upon closing the roof of the chamber warrants further investigation.

4.3 CLS and PTRMS Instruments

The CLS and PTRMS data were used here as reference guideline for the measurements and not for scrutinizing the performance
360 of the respective instruments. Nevertheless, some discrepancies between IBBCEAS, CLS and PTRMS were noted and are outlined here.

CLS: Mixing ratios of NO_2 measured by CLS and IBBCEAS frequently appeared to differ somewhat during the humidification of the dark chamber. The CLS instrument appears to systematically record higher NO_2 mixing ratios than IBBCEAS upon
365 humidification of an initially clean chamber without the obvious presence of NO_2. Examples of the observed behavior are shown in Figure 5 (see also Figure S8).

<p style="text-align:center">Figure 5</p>

There are two possible scenarios that may explain these observations: (a) It could be an artefact in the chemiluminescence device, which may be due to a surface effect of the blue light converter (BLC). Switching from a dry to a humidified chamber
370 leads to a severe change in the surface conditions of the BLC, which releases either NO or a substance that mimics an NO signal for some time until a new equilibrium has been reached. This type of behavior has occurred before in measurement campaigns at SAPHIR, where small temporary discrepancies between model calculations and measurement were observed. The nature of the potentially released substance is unclear. HONO would be more likely to stick to the walls rather than to be released unless heterogenous reactions are at play leading to the formation of NO. The effect is transient and vanishes after a
375 short time. The fact that rapidly changing water vapor concentrations can affect the instrumental background of CLS detectors and lead to a non-trivial memory effect that cannot be easily corrected retrospectively has also been reported recently in the

literature (Nussbaumer et al. 2021). (b) A small contamination of the milli-Q water and differences in the sample quality used for humidification cannot be fully ruled out. Those contaminations have also been observed before. The increase in the NO_2 signal upon humidification is supported by a significant increase in the NO signal (~120 pptv) observed by CLS. However, on

380 10 June 2011 this increase seems to be over after ca. 15 min while the humidification is still ongoing. The reason why the IBBCEAS instrument does not detect the increase in NO_2 if it is due to contamination is also unclear.

PTRMS: After introduction of MACR to the chamber on 11 July, initially higher mixing ratios were recorded by PTRMS rather than by IBBCEAS (between 11:50 hrs and ca. 15:30 hrs). The mixing ratios measured with the two instrument gradually

385 approach very similar values over the said time period until they agree rather well when the roof of the chamber was closed. The reason for this behavior is not clear since no obvious interference in this period was obvious.

4.4 Correlation of Data Obtained by Different Instrumental Methods

For the combined data sets of the instrument intercomparisons an overall good agreement for both trend and absolute mixing

390 ratios was observed between IBBCEAS and the established instruments at SAPHIR as illustrated in the correlation plots in Figures 6 and Table 1 (see also Figs. 1-3). The best agreement is observed on 5 Oct 2011 for both HONO and NO_2, which may be attributed to the fact that the least amount of interfering species were present in the chamber at that time. R coefficients range from 0.930 to 0.994 for HONO and between 0.937 and 0.992 for NO_2. An R coefficient of 0.962 is found for the single measurement of MACR.

5 Conclusion

395

In 2011 an incoherent broadband open-path cavity-enhanced absorption spectroscopy (IBBCEAS) instrument was established at the SAPHIR chamber in Jülich and optimized for the detection of HONO and NO_2 in the near UV region (352-386 nm) using a bright hot-spot Xe-arc lamp and a UV-enhanced CCD detector. Based on an effective reflectivity of $0.9978 < R_{eff} < 0.9986$ and a 20 m open-path cavity a 2σ detection limit of 26 pptv for HONO and 76 pptv for NO_2 was achieved for an

400 integration time of 1 min. Methacrolein was also detected at mixing ratios below 5 ppbv. These are highly competitive detection limits in comparison to those reported in the recent literature. The IBBCEAS instrument's performance for HONO and NO_2 detection was compared to that of long-path absorption photometry (LOPAP) and chemiluminescent NO_X detection, with R coefficients range from 0.930 to 0.994 for HONO, and between 0.937 and 0.992 for NO_2, respectively. At low concentrations however, and especially upon humidification of the chamber, a small temporary water interference on NO_2 mixing ratios were

405 observed in CLS measurements which was not observed in the IBBCEAS data.

6 Acknowledgement

SD gratefully acknowledges support through an INSPIRE post-doctoral fellowship by the Irish Research Council for Science Engineering and Technology which was cofounded by the Marie Curie actions, COFUND, under the Seventh European Framework Programme (FP7). We thank Andreas Wahner, Director of the Institute for Energy and Climate Research: Troposphere (IEK-8) at the Research Center in Jülich (Germany), and the team running the SAPHIR chamber, especially Ralf Tillmann, for providing the PTRMS data for this publication. The extraordinary craftsmanship of the mechanical workshop at Jülich in the context of this project is also gratefully recognized.

References

Acker, K., Möller, D., Wieprecht, W., Meixner, F. X., Bohn, B., Gilge, S., Plass-Dülmer, C., and Berresheim, H.: Strong daytime production of OH from HNO_2 at a rural mountain site, Geophys. Res. Lett., 33, L02809, doi: 10.1029/2005GL024643, 2006.

Alicke, B., Geyer, A., Hofzumahaus, A., Holland, F., Konrad, S., Patz, H. W., Schäfer, J., Stutz, J., Volz-Thomas, A., and Platt, U.: OH formation by HONO photolysis during the BERLIOZ experiment, J. Geophys. Res., 108, D4, doi: 10.1029/2001JD000579, 2003.

Ashu-Ayem, E. R., Nitschke, U., Monahan, C., Chen, J., Darby, S. B., Smith, P. D., O'Dowd, C. D., Stengel, D. B., and Venables, D. S.: Coastal iodine emissions. 1. Release of I_2 by *Laminaria Digitata* in chamber experiments, Environ. Sci. Tech., 46, 10413-10421, doi: 10.1021/es204534v, 2012.

Aumont, B., Chervier, F., and Laval, S.: Contribution of HONO sources to the $NO_X/HO_X/O_3$ chemistry in the polluted boundary layer, Atmos. Environ., 37, 487-498, doi: 10.1016/S1352-2310(02)00920-2, 2003.

Barney, W. S., Wingen, L. M., Lakin, M. J., Brauers, T., Stutz, J., and Finlayson-Pitts, B. J.: Infrared absorption cross-section measurements for nitrous acid (HONO) at room temperature, J. Phys. Chem. A, 104, 1692-1699, doi: 10.1021/jp010734d, 2000.

Beine, H. J., Amoroso, A., Esposito, G., Sparapani, R., Ianniello, A., Georgiadis, T., Nardino, M., Bonasoni, P., Cristofanelli, P., and Dominé, F.: Deposition of atmospheric nitrous acid on alkaline snow surfaces, Geophys. Res. Lett., 32, L10808, doi: 10.1029/2005GL022589, 2005.

Bitter, M., Ball, S. M., Povey, I. M., and Jones, R. L.: A broadband cavity ringdown spectrometer for in-situ measurements of atmospheric trace gases, Atmos. Chem. Phys., 5, 2547-2560, doi: 10.5194/acp-5-2547-2005, 2005.

Bottorff, B., Reidy, E., Mielke, L., Dusanter, S., and Stevens, P. S.: Development of a laser-photofragmentation laser-induced fluorescence instrument for the detection of nitrous acid and hydroxyl radicals in the atmosphere, Atmos. Meas. Tech., 14, 6039-6056, doi: 10.5194/amt-14-6039-2021, 2021.

Bröske, R., Kleffmann, J., and Wiesen, P.: Heterogeneous conversion of NO$_2$ on secondary organic aerosol surfaces: A possible source of nitrous acid (HONO) in the atmosphere? Atmos. Chem. Phys., 3, 469-474, doi: 10.5194/acp-3-469-2003, 2003.

Calvert, J. G., Yarwood, G., and Dunker, A. M.: An evaluation of the mechanism of nitrous acid formation in the urban
440   atmosphere, Res. Chem. Intermed., 20, 463-502, doi: 10.1163/156856794X00423, 1994.

Chen, J., Wenger, J. C., and Venables, D. S.: Near-ultraviolet absorption cross sections of nitrophenols and their potential influence on tropospheric oxidation capacity, J. Phys. Chem. A, 115, 12235-12242, 10.1021/jp206929r, 2011.

Dixneuf, S., Ruth, A. A., Vaughan, S., Varma, R. M., and Orphal, J.: The time dependence of molecular iodine emission from *Laminaria digitata*, Atmos. Chem. Phys., 9, 823-829, doi: 10.5194/acp-9-823-2009, 2009.

445 Djehiche, M., Tomas, A., Fittschen, C., and Coddeville, P.: First direct detection of HONO in the reaction of methylnitrite (CH$_3$ONO) with OH radicals, Environ. Sci. Tech., 45, 608-614, doi: 10.1021/es103076e, 2011.

Donaldson, M. A., Berke, A. E., and Raff, J. D.: Uptake of gas phase nitrous acid onto boundary layer soil surfaces, Environ. Sci. Tech., 48, 375-383, doi: 10.1021/es404156a, 2014.

Dorn, H. P., Apodaca, R. L., Ball, S. M., Brauers, T., Brown, S. S., Crowley, J. N., Dubé, W. P., Fuchs, H., Häseler, R.,
450   Heitmann, U., Jones, R. L., Kiendler-Scharr, A., Labazan, I., Langridge, J. M., Meinen, J., Mentel, T. F., Platt, U., Pöhler, D., Rohrer, F., Ruth, A. A., Schlosser, E., Schuster, G., Shillings, A. J. L., Simpson, W. R., Thieser, J., Tillmann, R., Varma, R., Venables, D. S., and Wahner, A.: Intercomparison of NO$_3$ radical detection instruments in the atmosphere simulation chamber SAPHIR, Atmos. Meas. Tech., 6, 1111-1140, doi: 10.5194/amt-6-1111-2013, 2013.

Duan, J., Qin, M., Ouyang, B., Fang, W., Li, X., Lu, K., Tang, K., Liang, S., Meng, F., Hu, Z., Xie, P., Liu, W., and Häseler,
455   R.: Development of an incoherent broadband cavity-enhanced absorption spectrometer for in situ measurements of HONO and NO$_2$, Atmos. Meas. Tech., 11, 4531-4543, doi: 10.5194/amt-11-4531-2018, 2018.

Febo, A., Perrino, C., and Allegrini, I.: Measurement of nitrous acid in Milan, Italy, by DOAS and diffusion denuders, Atmos. Environ., 30, 3599-3609, doi: 10.1016/1352-2310(96)00069-6, 1996.

Ferm, M., and Sjödin, A.: A sodium carbonate coated denuder for determination of nitrous acid in the atmosphere, Atmos.
460   Environ., 19, 979-983, doi: 10.1016/0004-6981(85)90243-4, 1985.

Fiedler, S. E., Hese, A., and Ruth, A. A.: Incoherent broad-band cavity-enhanced absorption spectroscopy, Chem. Phys. Lett., 371, 284-294, doi: 10.1016/S0009-2614(03)00263-X, 2003.

Finlayson-Pitts, B. J., Wingen, L. M., Sumner, A. L., Syomin, D., and Ramazan, K. A.: The heterogeneous hydrolysis of NO$_2$ in laboratory systems and in outdoor and indoor atmospheres: An integrated mechanism, Phys. Chem. Chem. Phys. 5,
465   223-242, doi: 10.1039/B208564J, 2003.

Fouqueau, A., Cirtog, M., Cazaunau, M., Pangui, E., Zapf, P., Siour, G., Landsheere, X., Méjean, G., Romanini, D., and Picquet-Varrault, B.: Implementation of an incoherent broadband cavity-enhanced absorption spectroscopy technique in an atmospheric simulation chamber for in situ NO$_3$ monitoring: characterization and validation for kinetic studies, Atmos. Meas. Tech., 13, 6311-6323, doi: 10.5194/amt-13-6311-2020, 2020.

470   Fuchs, H., Ball, S. M., Bohn, B., Brauers, T., Cohen, R. C., Dorn, H.-P., Dubé, W. P., Fry, J. L., Häseler, R., Heitmann, U., Jones, R. L., Kleffmann, J., Mentel, T. F., Müsgen, P., Rohrer, F., Rollins, A. W., Ruth, A. A., Kiendler-Scharr, A., Schlosser, E., Shillings, A. J. L., Tillmann, R., Varma, R. M., Venables, D. S., Villena Tapia, G., Wahner, A., Wegener, R., Wooldridge, P. J., and Brown, S. S.: Intercomparison of measurements of NO_2 concentrations in the atmosphere simulation chamber SAPHIR during the NO3Comp campaign, Atmos. Meas. Tech., 3, 21-37, doi: 10.5194/amt-3-21-

475   2010, 2010.

Fuchs, H., Acir, I. H., Bohn, B., Brauers, T., Dorn, H.-P., Häseler, R., Hofzumahaus, A., Holland, F., Kaminski, M., Li, X., Lu, K., Lutz, A., Nehr, S., Rohrer, F., Tillmann, R., Wegener, R., and Wahner, A.: OH regeneration from methacrolein oxidation investigated in the atmosphere simulation chamber SAPHIR, Atmos. Chem. Phys., 14, 7895-7908, doi: 10.5194/acp-14-7895-2014, 2014.

480   Gherman, T., Venables, D. S., Vaughan, S., Orphal, J., and Ruth, A. A.: Incoherent broadband cavity-enhanced absorption spectroscopy in the near-ultraviolet: Application to HONO and NO_2, Environ. Sci. Tech., 42, 890-895, doi: 10.1021/es0716913, 2008.

Häseler, R., Brauers, T., Holland, F., and Wahner, A.: Development and application of a new mobile LOPAP instrument for the measurement of HONO altitude profiles in the planetary boundary layer, Atmos. Meas. Tech. Discuss., 2, 2027-
485   2054, doi: 10.5194/amtd-2-2027-2009, 2009.

Hanst, P. L., Wong, N. W., and Bragin, J.: A long-path infrared study of Los Angeles smog, Atmos. Environ., 16, 969-981, doi: 10.1016/0004-6981(82)90183-4, 1982.

Harrison, R. M., and Kitto, A. M. N.: Evidence for a surface source of atmospheric nitrous acid, Atmos. Environ., 28, 1089-1094, doi: 10.1016/1352-2310(94)90286-0, 1994.

490   Heland, J., Kleffmann, J., Kurtenbach, R., and Wiesen, P.: A new instrument to measure gaseous nitrous acid (HONO) in the atmosphere, Environ. Sci. Tech., 35, 3207-3212, doi: 10.1021/es000303t, 2001.

Hoch, D. J., Buxmann, J., Sihler, H., Pöhler, D., Zetzsch, C., and Platt, U.: A cavity-enhanced differential optical absorption spectroscopy instrument for measurement of BrO, HCHO, HONO and O_3, Atmos. Meas. Tech. Discuss., 5, 3079-3115, doi: 10.5194/amtd-5-3079-2012, 2012.

495   Huang, G., Zhou, X. L., Deng, G. H., Qiao, H. C., and Civerolo, K.: Measurements of atmospheric nitrous acid and nitric acid, Atmos. Environ., 36, 2225-2235, doi: 10.1016/S1352-2310(02)00170-X, 2002.

Jain, C., Morajkar, P., Schoemaecker, C., Viskolcz, B., and Fittschen, C.: Measurement of absolute absorption cross sections for nitrous acid (HONO) in the near-infrared region by the continuous wave cavity ring-down spectroscopy (cw-CRDS) technique coupled to laser photolysis, J. Phys. Chem. A, 115, 10720-10728, doi: 10.1021/jp203001y, 2011.

500   Johnston, H. S., and Graham, R.: Photochemistry of NO_x and HNO_x compounds, Can. J. Chem.-Rev. Can. Chim., 52, 1415-1423, doi: 10.1139/v74-214, 1974.

Jordan, N., and Osthoff, H. D.: Quantification of nitrous acid (HONO) and nitrogen dioxide (NO₂) in ambient air by broadband cavity-enhanced absorption spectroscopy (IBBCEAS) between 361–388 nm, Atmos. Meas. Tech., 13, 273-285, doi: 10.5194/amt-13-273-2020, 2020.

505 Karl, M.: Modellierung atmosphärisch-chemischer Reaktionen in der Tageslicht-Atmosphären-Simulationskammer SAPHIR, Dissertation, Westfälische Wilhelms-Universität Münster, 2004.

Kleffmann, J., Heland, J., Kurtenbach, R., Lorzer, J., and Wiesen, P.: A new instrument (LOPAP) for the detection of nitrous acid (HONO), Environ. Sci. Pollut. Res., 4, 48-54, doi: 10.1021/es000303t, 2002.

Kleffmann, J., Kurtenbach, R., Lorzer, J., Wiesen, P., Kalthoff, N., Vogel, B., and Vogel, H.: Measured and simulated vertical
510 profiles of nitrous acid - Part I: Field measurements, Atmos. Environ., 37, 2949-2955, doi: 10.1016/S1352-2310(03)00242-5, 2003.

Kleffmann, J., Gavriloaiei, T., Hofzumahaus, A., Holland, F., Koppmann, R., Rupp, L., Schlosser, E., Siese, M., and Wahner, A.: Daytime formation of nitrous acid: A major source of OH radicals in a forest, Geophys. Res. Lett. – Atmos. Sci., 32, L05818, doi: 10.1029/2005GL022524, 2005.

515 Kleffmann, J., Lörzer, J. C., Wiesen, P., Kern, C., Trick, S., Volkamer, R., Rodenas, M., and Wirtz, K.: Intercomparison of the DOAS and LOPAP techniques for the detection of nitrous acid (HONO), Atmos. Environ., 40, 3640-3652, doi: 10.1016/j.atmosenv.2006.03.027, 2006.

Kleffmann, J.: Daytime sources of nitrous acid (HONO) in the atmospheric boundary layer, Chem. Phys. Chem., 8, 1137-1144, doi: 10.1002/cphc.200700016, 2007.

520 Lammel, G., and Cape, J. N.: Nitrous acid and nitrite in the atmosphere, Chem. Soc. Rev., 25, 361-369, doi: 10.1039/CS9962500361, 1996.

Langridge, J. M., Ball, S. M., and Jones, R. L.: A compact broadband cavity enhanced absorption spectrometer for detection of atmospheric NO₂ using light emitting diodes, Analyst, 131, 916-922, doi: 10.1039/B605636A, 2006.

Leigh, R. J., Ball, S. M., Whitehead, J., Leblanc, C., Shillings, A. J. L., Mahajan, A. S., Oetjen, H., Lee, J. D., Jones, C. E.,
525 Dorsey, J. R., Gallagher, M., Jones, R. L., Plane, J. M. C., Potin, P., and McFiggans, G.: Measurements and modelling of molecular iodine emissions, transport and photodestruction in the coastal region around Roscoff, Atmos. Chem. Phys., 10, 11823-11838, doi: 10.5194/acp-10-11823-2010, 2010.

Li, X., Brauers, T., Häseler, R., Bohn, B., Fuchs, H., Hofzumahaus, A., Holland, F., Lou, S., Lu, K. D., Rohrer, F., Hu, M., Zeng, L. M., Zhang, Y. H., Garland, R. M., Su, H., Nowak, A., Wiedensohler, A., Takegawa, N., Shao, M., and Wahner,
530 A.: Exploring the atmospheric chemistry of nitrous acid (HONO) at a rural site in Southern China, Atmos. Chem. Phys., 12, 1497-1513, doi: 10.5194/acp-12-1497-2012, 2012.

Li, X., Rohrer, F., Hofzumahaus, A., Brauers, T., Häseler, R., Bohn, B., Broch, S., Fuchs, H., Gomm, S., Holland, F., Jäger, J., Kaiser, J., Keutsch, F. N., Lohse, I., Lu, K. D., Tillmann, R., Wegener, R., Wolfe, G. M., Mentel, T. F., Kiendler-Scharr, A., and Wahner, A.: Missing gas-phase source of HONO inferred from zeppelin measurements in the
535 troposphere, Science, 344, 292-296, doi: 10.1126/science.1248999, 2014.

Liao, W., Hecobian, A., Mastromarino, J., and Tan, D.: Development of a photo-fragmentation/laser-induced fluorescence measurement of atmospheric nitrous acid, Atmos. Environ., 40, 17-26, doi: 10.1016/j.atmosenv.2005.07.001, 2006.

Liu, Y., Nie, W., Xu, Z., Wang, T., Wang, R., Li, Y., Wang, L., Chi, X., and Ding, A.: Contributions of different sources to nitrous acid (HONO) at the SORPES station in eastern China: results from one-year continuous observation, Atmos.
540   Chem. Phys. Discuss., doi: 10.5194/acp-2019-219, (in review), 2019.

Meller, R., private communication to, Röth, E.-P., Ruhnke, R., Moortgat, G., and Schneider, W., 1990 (spectral resolution 0.01 nm, T = 294 K); in: Keller-Rudek, H., Moortgat, G. K., Sander, R., and Sörensen, R.: *The MPI-Mainz UV/VIS spectral atlas of gaseous molecules of atmospheric interest,* Earth Syst. Sci. Data, 5, 365-373, doi: 10.5194/essd-5-365-2013, 2013.

545 Mérienne, M. F., Jenouvrier, A., and Coquart, B.: The NO_2 absorption-spectrum. 1. Absorption cross-sections at ambient-temperature in the 300-500 nm region, J. Atmos. Chem., 20, 281-297, doi: 10.1007/BF00694498, 1995.

Min, K. E., Washenfelder, R. A., Dubé, W. P., Langford, A. O., Edwards, P. M., Zarzana, K. J., Stutz, J., Lu, K., Rohrer, F., Zhang, Y., and Brown, S. S.: A broadband cavity enhanced absorption spectrometer for aircraft measurements of glyoxal, methylglyoxal, nitrous acid, nitrogen dioxide, and water vapor, Atmos. Meas. Tech., 9, 423-440, doi:
550   10.5194/amt-9-423-2016, 2016.

Nakashima, Y., and Sadanaga, Y.: Validation of in situ measurements of atmospheric nitrous acid using incoherent broadband cavity-enhanced absorption spectroscopy, Analyst. Sci., 33, 519-524, doi: 10.2116/analsci.33.519, 2017.

Nehr, S., Bohn, B., Dorn, H. P., Fuchs, H., Häseler, R., Hofzumahaus, A., Li, X., Rohrer, F., Tillmann, R., and Wahner, A.: Atmospheric photochemistry of aromatic hydrocarbons: OH budgets during SAPHIR chamber experiments, Atmos.
555   Chem. Phys., 14, 6941-6952, doi: 10.5194/acp-14-6941-2014, 2014.

Nussbaumer, C. M., Parchatka, U., Tadic, I., Bohn, B., Marno, D., Martinez, M., Rohloff, R., Harder, H., Kluge, F., Pfeilsticker, K., Obersteiner, F., Zöger, M., Doerich, R., Crowley, J. N., Lelieveld, J., and Fischer, H.: New photolytic converter for improving aircraft measurements of NO_2 via chemiluminescence, Atmos. Meas. Tech. Discuss. [preprint in review], doi: 10.5194/amt-2021-180, 2021.

560 Oms, M. T., Jongejan, P. A. C., Veltkamp, A. C., Wyers, G. P., and Slanina, J.: Continuous monitoring of atmospheric HCl, HNO_2, HNO_3, and SO_2, by wet-annular denuder air sampling with on-line chromatographic analysis, Int. J. Environ. Anal. Chem., 62, 207-218, doi: 10.1080/03067319608028134, 1996.

Press, W. H., Flannery, T. S. and Vetterling, W. T.: Numerical Recipes: The Art of Scientific Computing, Cambridge U. Press, 1986, pp. 51 and 670.

565 Ramazan, K. A., Syomin, D., and Finlayson-Pitts, B. J.: The photochemical production of HONO during the heterogeneous hydrolysis of NO_2, Phys. Chem. Chem. Phys., 6, 3836-3843, doi: 10.1039/B402195A, 2004.

Reisinger, A. R.: Observations of HNO_2 in the polluted winter atmosphere: possible heterogeneous production on aerosols. Atmos. Environ., 34, 3865-3874, doi: 10.1016/S1352-2310(00)00179-5, 2000.

Roberts, J. M., and Bertman, S. B.: The thermal decomposition of peroxy acetic nitric anhydride (PAN) and peroxymethacrylic nitric anhydride (MPAN), Int. J. Chem. Kinetics, 24, 297-307, doi: 10.1002/kin.550240307, 1992.

Rodenas, M., Munoz, A., Alacreu, F., Brauers, T., Dorn, H. P., Kleffmann, J., and Bloss, W.: Assessment of HONO Measurements: The FIONA Campaign at EUPHORE, in: *Disposal of Dangerous Chemicals in Urban Areas and Mega Cities: Role of Oxides and Acids of Nitrogen in Atmospheric Chemistry*, Eds. Barnes, I., and Rudzinski, K. J., Springer, Dordrecht, pp. 45-58, 2013.

Rodgers, M. O., and Davis, D. D.: A UV-photofragmentation laser-induced fluorescence sensor for detection of HONO, Environ. Sci. Tech., 23, 1106-1112, doi: 10.1021/es00067a007, 1989.

Rohrer, F., and Brüning, D.: Surface NO and NO_2 mixing ratios measured between 30 degrees-N and 30 degrees-S in the Atlantic region, J. Atmos. Chem., 15, 253-267, doi: 10.1007/BF00115397, 1992.

Rohrer, F., Bohn, B., Brauers, T., Bruning, D., Johnen, F. J., Wahner, A., and Kleffmann, J.: Characterisation of the photolytic HONO-source in the atmosphere simulation chamber SAPHIR, Atmos. Chem. Phys., 5, 2189-2201, doi: 10.5194/acp-5-2189-2005, 2005.

Ruth, A. A., Dixneuf, S., Raghunandan, R.: Broadband cavity-enhanced absorption Spectroscopy with incoherent light, in: *Cavity enhanced spectroscopy and sensing*, Eds. Gagliardi, G., and Loock, H. P., Springer Series in Optical Sciences, 179, 485-517, doi: 10.1007/978-3-642-40003-2., 2014.

Saiz-Lopez, A., Plane, J. M. C., McFiggans, G., Williams, P. I., Ball, S. M., Bitter, M., Jones, R. L., Hongwei, C., and Hoffmann, T.: Modelling molecular iodine emissions in a coastal marine environment: the link to new particle formation, Atmos. Chem. Phys., 6, 883-895, doi: 10.5194/acp-6-883-2006, 2006.

Schiller, C. L., Locquiao, S., Johnson, T. J., and Harris, G. W.: Atmospheric measurements of HONO by tunable diode laser absorption spectroscopy, J. Atmos. Chem., 40, 275-293, doi: 10.1023/A:1012264601306, 2001.

Scharko, N. K., Berke, A. E., and Raff, J. D.: Release of nitrous acid and nitrogen dioxide from nitrate photolysis in acidic aqueous solutions, Environ. Sci. Tech., 48, 11991-12001, doi: 10.1021/es503088x, 2014.

Simon, P. K., and Dasgupta, P. K.: Continuous automated measurement of gaseous nitrous and nitric acids and particulate nitrite and nitrate, Environ. Sci. Tech., 29, 1534-1541, doi: 10.1021/es00006a015, 1995.

Spataro, F., and Ianniello, A.: Sources of atmospheric nitrous acid: State of the science, current research needs, and future prospects, J. Air Waste Man. Assoc., 64, 1232-1250, doi: 10.1080/10962247.2014.952846, 2014.

Spindler, G., Hesper, J., Brüggemann, E., Dubois, R., Müller, T., and Herrmann, H.: Wet annular denuder measurements of nitrous acid: laboratory study of the artefact reaction of NO_2 with S(IV) in aqueous solution and comparison with field measurements, Atmos. Environ., 37, 2643-2662, doi: 10.1016/S1352-2310(03)00209-7, 2003.

Staffelbach, T., Neftel, A., and Horowitz, L. W.: Photochemical oxidant formation over southern Switzerland. 2. Model results, J. Geophys. Res.-Atmos., 102, 23363-23373, doi: 10.1029/97JD00932, 1997.

Stemmler, K., Ammann, M., Donders, C., Kleffmann, J., and George, C.: Photosensitized reduction of nitrogen dioxide on humic acid as a source of nitrous acid, Nature, 440, 195-198, doi: 10.1038/nature04603, 2006.

Stutz, J., Kim, E. S., Platt, U., Bruno, P., Perrino, C., and Febo, A.: UV-visible absorption cross sections of nitrous acid, J. Geophys. Res.-Atmos., 105, 14585-14592, doi: 10.1029/2000JD900003, 2000.

605   Stutz, J., Oha, H.-J., Whitlow, S. I., Anderson, C., Dibb, J. E., Flynn, J. H., Rappenglück, B., and Lefer, B.: Simultaneous DOAS and mist-chamber IC measurements of HONO in Houston, TX, Atmos. Environ., 44, 4090-4098, doi: 10.1016/j.atmosenv.2009.02.003, 2010.

Takenaka, N., Terada, H., Oro, Y., Hiroi, M., Yoshikawa, H., Okitsu, K., and Bandow, H.: A new method for the measurement of trace amounts of HONO in the atmosphere using an air-dragged aqua-membrane-type denuder and fluorescence
610   detection, Analyst, 129, 1130-1136, doi: 10.1039/B407726A, 2004.

Thalman, R., and Volkamer, R.: Inherent calibration of a blue LED-CE-DOAS instrument to measure iodine oxide, glyoxal, methyl glyoxal, nitrogen dioxide, water vapour and aerosol extinction in open cavity mode, Atmos. Meas. Tech., 3, 1797-1814, doi: 10.5194/amt-3-1797-2010, 2010.

Varma, R. M., Venables, D. S., Ruth, A. A., Heitmann, U., Schlosser, E., and Dixneuf, S.: Long optical cavities for open-path
615   monitoring of atmospheric trace gases and aerosol extinction, Appl. Opt., 48, B159-B171, doi: 10.1364/AO.48.00B159, 2009.

Varma, R. M., Ball, S. M., Brauers, T., Dorn, H. P., Heitmann, U., Jones, R. L., Platt, U., Pöhler, D., Ruth, A. A., Shillings, A. J. L., Thieser, J., Wahner, A., and Venables, D. S.: Light extinction by secondary organic aerosol: an intercomparison of three broadband cavity spectrometers, Atmos. Meas. Tech., 6, 3115-3130, doi: 10.5194/amt-6-3115-2013, 2013.

620   Vogel, B., Vogel, H., Kleffmann, J., and Kurtenbach, R.: Measured and simulated vertical profiles of nitrous acid - Part II. Model simulations and indications for a photolytic source, Atmos. Environ., 37, 2957-2966, doi: 10.1016/S1352-2310(03)00243-7, 2003.

Wang, L. M., and Zhang, J. S.: Detection of nitrous acid by cavity ring down spectroscopy, Environ. Sci. Tech., 34, 4221-4227, doi: 10.1021/es0011055, 2000.

625   Washenfelder, R. A., Langford, A. O., Fuchs, H., and Brown, S. S.: Measurement of glyoxal using an incoherent broadband cavity enhanced absorption spectrometer, Atmos. Chem. Phys., 8, 7779-7793, doi: 10.1021/es0011055, 2008.

Wisthaler, A., Apel, E. C., Bossmeyer, J., Hansel, A., Junkermann, W., Koppmann, R., Meier, R., Müller, K., Solomon, S. J., Steinbrecher, R., Tillmann, R., and Brauers, T.: Technical Note: Intercomparison of formaldehyde measurements at the atmosphere simulation chamber SAPHIR, Atmos. Chem. Phys., 8, 2189-2200, doi: 10.5194/acp-8-2189-2008,
630   2008.

Wu, T., Zhao, W., Chen, W., Zhang, W., and Gao, X.: Incoherent broadband cavity enhanced absorption spectroscopy for in situ measurements of NO_2 with a blue light emitting diode, Appl. Phys. B - Lasers and Optics, 94, 85-94, doi: 10.1007/s00340-008-3308-8, 2009.

Wu, T., Chen, W., Fertein, E., Cazier, F., Dewaele, D., and Gao, X.: Development of an open-path incoherent broadband
635   cavity-enhanced spectroscopy based instrument for simultaneous measurement of HONO and NO_2 in ambient air, Appl. Phys. B - Lasers and Optics, 106, 501-509, doi: 10.1007/s00340-011-4818-3, 2012.

Yi, H., Cazaunau, M., Gratien, A., Michoud, V., Pangui, E., Doussin, J.-F., and Chen, W.: Intercomparison of IBBCEAS, NitroMAC and FTIR analyses for HONO, NO_2 and CH_2O measurements during the reaction of NO_2 with H_2O vapour in the simulation chamber CESAM, Atmos. Meas. Tech., 14, 5701-5715, doi: 10.5194/amt-14-5701-2021, 2021.

640 Zhou, X. L., Civerolo, K., Dai, H. P., Huang, G., Schwab, J., and Demerjian, K.: Summertime nitrous acid chemistry in the atmospheric boundary layer at a rural site in New York state, J. Geophys. Res.-Atmos., 107, D21.4590, doi: 10.1029/2001JD001539, 2002a.

Zhou, X. L., He, Y., Huang, G., Thornberry, T. D., Carroll, M. A., and Bertman, S. B.: Photochemical production of nitrous acid on glass sample manifold surface, Geophys. Res. Lett., 29, 1681, doi: 10.1029/2002GL015080, 2002b.

645 Zhou, X. L., Gao, H. L., He, Y., Huang, G., Bertman, S. B., Civerolo, K., and Schwab, J.: Nitric acid photolysis on surfaces in low-NOx environments: Significant atmospheric implications, Geophys. Res. Lett., 30, 23.2217, doi: 10.1029/2003GL018620, 2003.

650

655

660

665

670

675

680

685 **Table 1. Comparison of correlation plot data. N: number of data points, a and b: regression coefficients, σ (a) and and σ (b): bootstrap errors of the linear square fit $y = a + bx$ (where y represent IBBCEAS data [pptv] and x the data [pptv] by either LOPAP, CLS or PTRMS), r^2: Pearson linear correlation coefficients.**

date	N	a [pptv]	σ(a) [pptv]	B	σ(b)	r^2
HONO: IBBCEAS vs. LOPAP						
11 July	553	11.1	2.5	0.915	0.013	0.8844
12 July	360	−0.3	1.3	0.883	0.017	0.8645
5 Oct	299	−16.2	1.1	0.992	0.007	0.9885
6 Oct	394	−26.1	2.9	1.020	0.013	0.9408
all 4 days	**1668**	**−8.4**	**0.9**	**0.973**	**0.005**	**0.9489**
NO$_2$: IBBCEAS vs. CLS						
11 July	708	−157	11	1.085	0.012	0.9253
12 July	378	−56	5	1.090	0.019	0.9415
5 Oct	531	15	7	1.050	0.011	0.9837
6 Oct	634	3	2	1.385	0.019	0.8786
all 4 days	**3011**	**−29**	**3**	**1.031**	**0.007**	**0.9700**
MACR: IBBCEAS vs. PTRMS						
11 July	657	103	27	0.947	0.010	0.9623

690
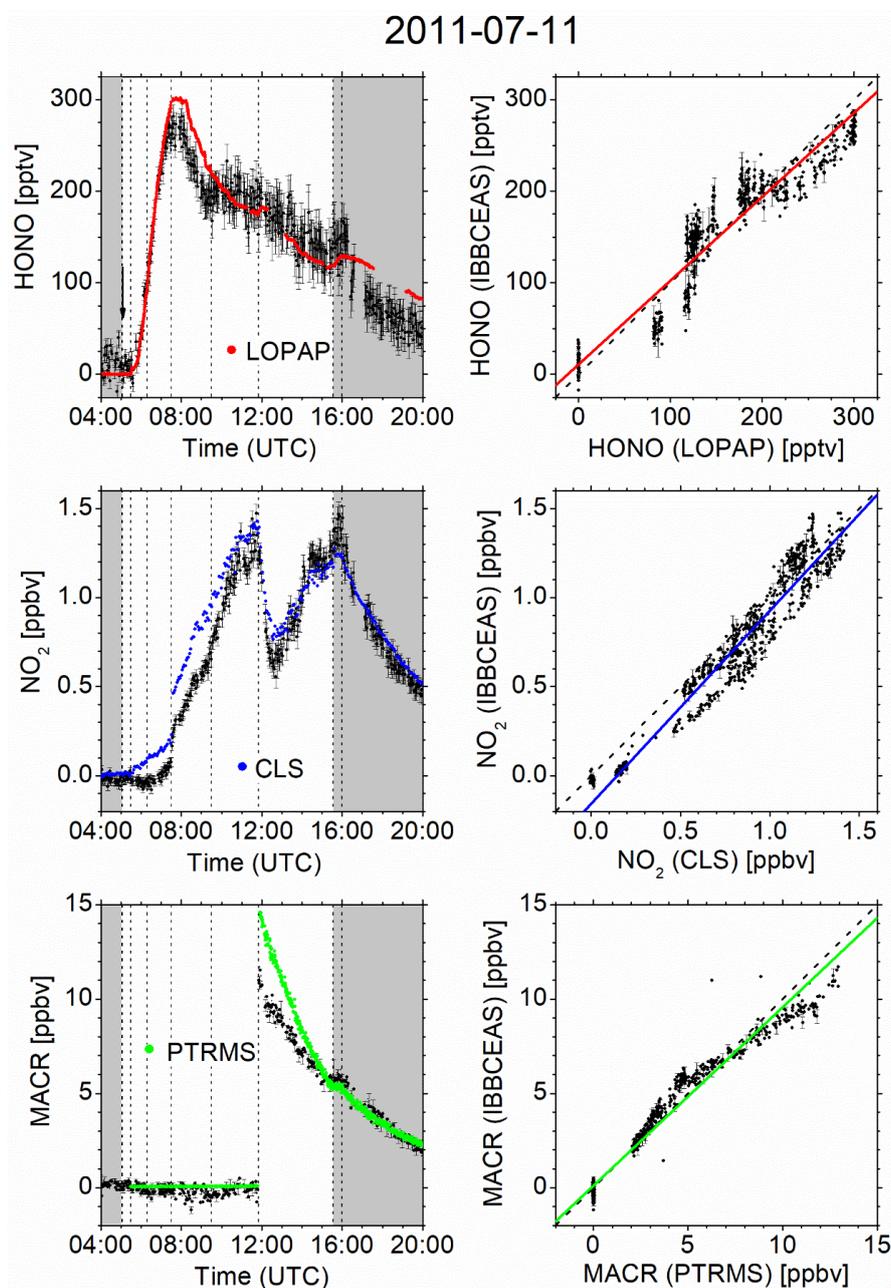
Figure 1: *Left panels:* **Time-dependent HONO, NO₂ and MACR mixing ratios measured by IBBCEAS (black trace) at SAPHIR on 11 July 2011. Dashed vertical lines indicate changes in the chamber conditions according to the experimental protocol: Overnight flushing of chamber with zero air stopped (5:03), roof opened (5:05), start of humidification (5:30), end of humidification (6:18), 40 ppbv O₃ (7:30), 750 ppbv CO (09:30), MACR (11:51), roof closing (15:33), flushing with zero air started (16:00). IBBCEAS data taken in the near-UV region of the spectrum (352-386 nm) are compared to LOPAP (red), CLS (blue) and PTRMS (green) data. The vertical black arrow indicates the time when I_0 was measured (generally for 10 min).** *Right panels:* **Correlation plots of two instruments being compared against IBBCEAS. The dashed line represents the identity, the colored solid lines are linear regressions to the data. Results are listed in Table 1.**

700
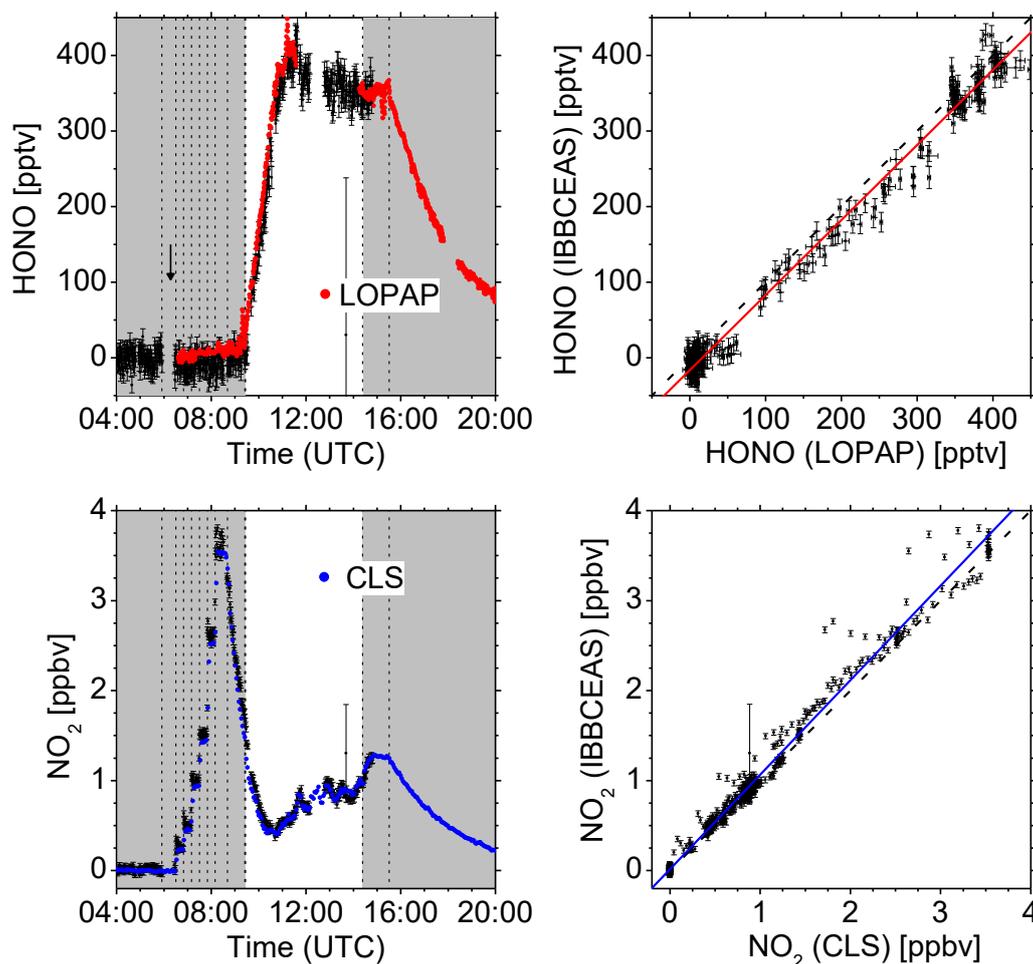
Figure 2: *Left panels:* **Time-dependent HONO and NO₂ mixing ratios measured at SAPHIR on 5 October 2011. Dashed vertical lines**
indicate changes in the chamber conditions according to the experimental protocol: Overnight flushing stopped (5:55), 250 pptv NO₂
(6:30 and 6:50), 500 pptv NO₂ (7:10 and 7:30), 1 ppbv NO₂ (7:50 and 8:10), start humidification (8:41), stop humidification (9:25),
roof opening (9:27), roof closing (14:23), flushing started (15:31). IBBCEAS data taken in the near-UV region of the spectrum (352-
386 nm) are compared to LOPAP (red) and CLS (blue). The vertical black arrow indicates the time when I_0 was measured (generally
for 10 min). *Right panels:* **Correlation plots of two instruments being compared against IBBCEAS. The dashed line represents the**
identity, the colored solid lines are linear regressions to the data. Results are listed in Table 1.
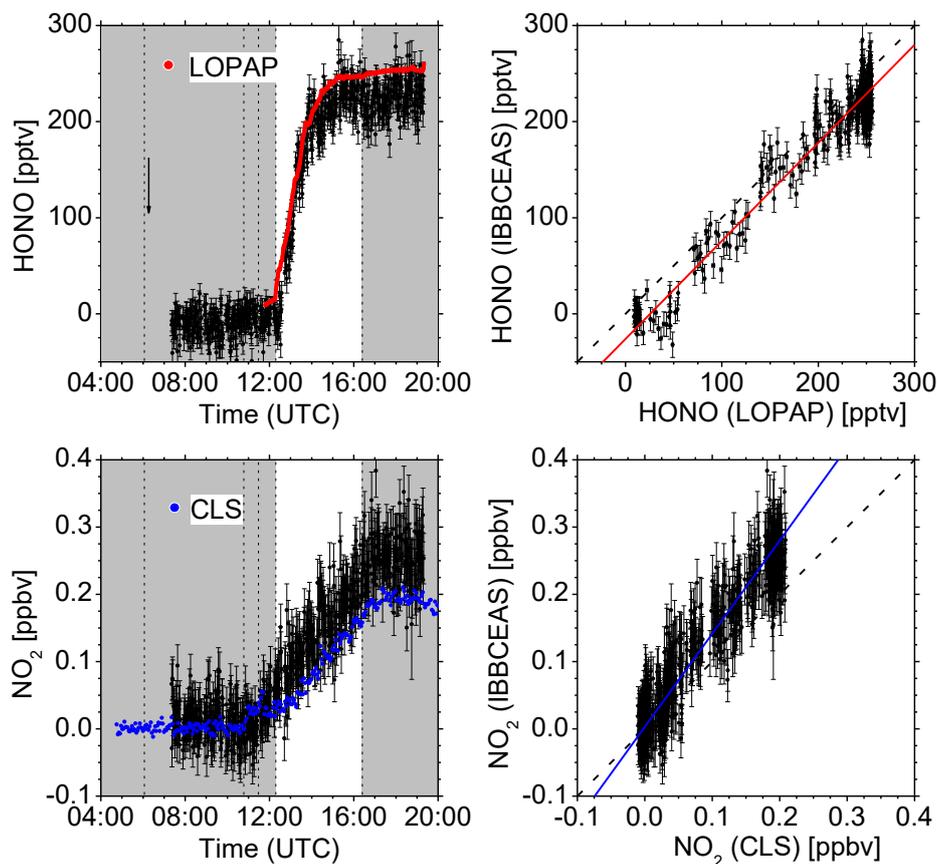
Figure 3: *Left panels:* **Time-dependent HONO and NO₂ mixing ratios measured at SAPHIR on 6 October 2011. Dashed vertical lines indicate changes in the chamber conditions according to the experimental protocol: Overnight flushing stopped (6:04), start humidification (10:47), stop humidification (11:29), roof opening (12:18), roof closing (16:24). IBBCEAS data taken in the near-UV region of the spectrum (352-386 nm) are compared to LOPAP (red) and CLS (blue) data. The vertical black arrow indicates the time when *I₀* was measured (generally for 10 min).** *Right panels:* **Correlation plots of two instruments being compared against IBBCEAS. The dashed line represents the identity, the colored solid lines are linear regressions to the data. Results are listed in Table 1.**
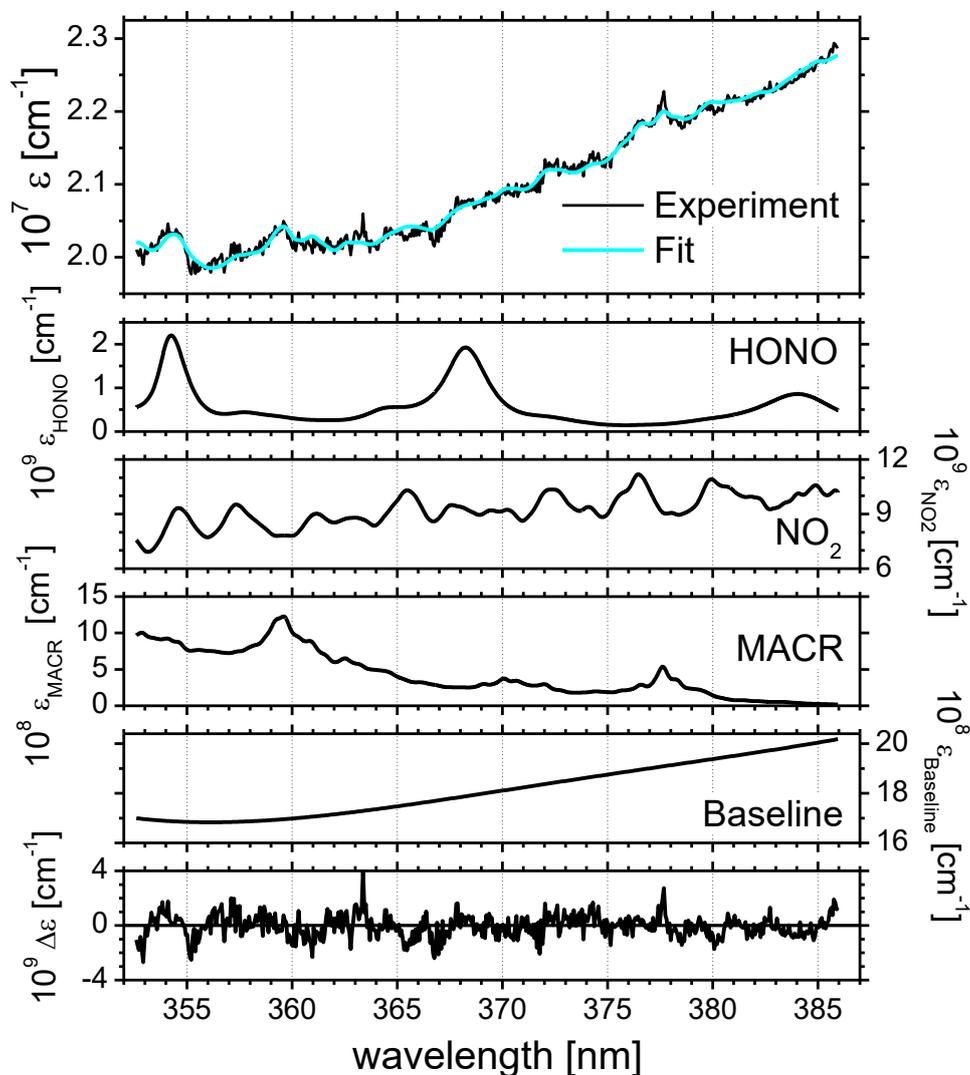
725

Figure 4: Example of the extinction coefficient spectrum, ε(λ), measured with IBBCEAS at SAPHIR in the wavelength range 352-386 nm with an integration time of 1 min, taken at 13:00 hrs on 11 July 2011. Uppermost panel: measured extinction (black), fit of eq (1) to the extinction (cyan). Lowermost panel: Absolute fit residuals $\Delta\varepsilon = \varepsilon_{fit} - \varepsilon_{exp}$. HONO, NO₂ and MACR mixing ratios were retrieved as $n_{HONO} = 0.160$ ppbv, $n_{NO2} = 0.586$ ppbv and $n_{MACR} = 8.055$ ppbv, respectively. The corresponding contributions and the

730 **polynomial baseline are shown in the middle panels. The absolute wavelength scale was calibrated with a low-pressure Ne pen ray lamp. O₂-O₂ absorption at ~360 and ~380 nm not relevant as evident from the residuals in the lowermost panel.**

735
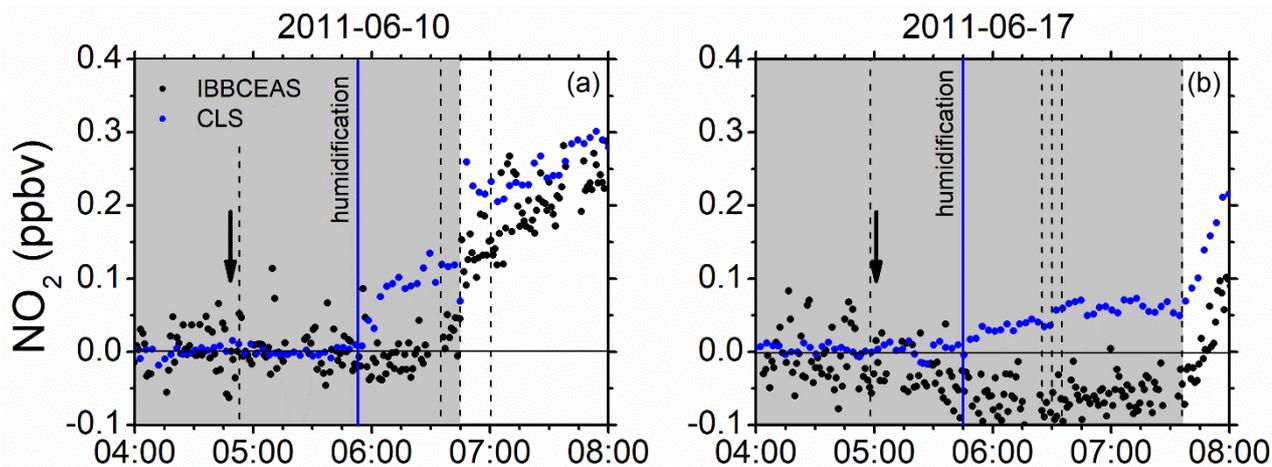
Figure 5: Examples of the small increase of NO₂ mixing ratios upon humidification in the *dark* chamber measured with CLS (blue dots) in comparison to those measured with IBBCEAS (black dots): (a) 10 June 2011: CO₂ addition (4:53), start of humidification (5:52 - vertical solid blue line), ozone addition (6:36), roof opened (6:46), isoprene addition (7:01). (b) 17 June 2011: Flushing of chamber stopped (04:58), start of humidification (05:45), end of humidification (06:25), O₃ addition (06:30) in dark chamber, CO addition (06:35), roof opened (07:36). Vertical solid arrows indicate the time of the zeroing measurement (*I*₀).

740

745
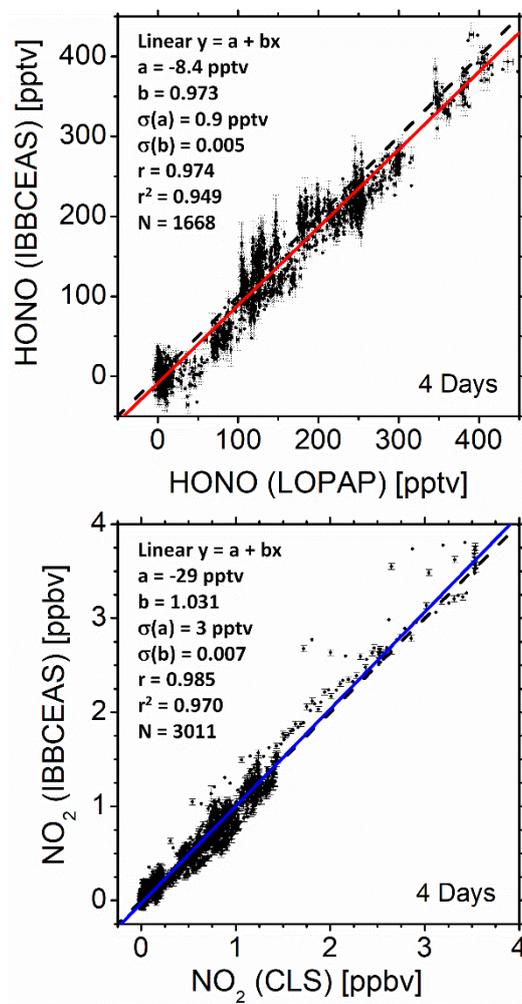
Figure 6: Correlation plots of two instruments of the entire data set from the intercomparison. The dashed line represents the identity, the coloured solid lines are linear regressions to the data (see also Table 1).